



OPEN

SUBJECT AREAS:

BIOMEDICAL
ENGINEERING

BIOMEDICAL MATERIALS

Received
23 July 2013Accepted
10 February 2014Published
18 March 2014Correspondence and
requests for materials
should be addressed to
G.K. (gkaur82@vt.
edu)

Synthesis, cytotoxicity, and hydroxyapatite formation in 27-Tris-SBF for sol-gel based $\text{CaO-P}_2\text{O}_5\text{-SiO}_2\text{-B}_2\text{O}_3\text{-ZnO}$ bioactive glasses

Gurbinder Kaur¹, G. Pickrell¹, G. Kimsawatde², D. Homa¹, H. A. Allbee¹ & N. Sriranganathan²¹Department of Material Science and Engineering, Holden Hall, Virginia Polytechnic Institute and State University, Blacksburg, Virginia-24060, USA, ²Department of Biomedical Sciences and Pathobiology, Virginia Polytechnic Institute and State University, Blacksburg, Virginia-24060, USA.

$\text{CaO-P}_2\text{O}_5\text{-SiO}_2\text{-B}_2\text{O}_3\text{-ZnO}$ bioactive glasses were prepared via an optimized sol-gel method. The current investigation was focused on producing novel zinc based calcium phosphoborosilicate glasses and to evaluate their mechanical, rheological, and biocompatible properties. The morphology and composition of these glasses were studied using X-ray diffraction (XRD) and scanning electron microscopy (SEM). The particle size, mechanical and flexural strength was also determined. Furthermore, the zeta potential of all the glasses were determined to estimate their flocculation tendency. The thermal analysis and weight loss measurements were carried out using differential scanning calorimetry (DSC) and thermogravimetric analysis (TGA) respectively. For assessing the in-vitro bioactive character of synthesized glasses, the ability for apatite formation on their surface upon their immersion in simulated body fluid (SBF) was checked using SEM and pH measurements. MTS assay cytotoxicity assay and live-dead cell viability test were conducted on J774A.1 cells murine macrophage cells for different glass concentrations.

Hench reported the first Bioglass 45S5 ($\text{SiO}_2\text{-Na}_2\text{O-CaO-P}_2\text{O}_5$) 40 years ago¹. Since then, many bioactive glass/glass ceramics have been developed for bone repair and grafts. Bioactive glasses have received special attention due to their unique characteristics like (i) flexible and property specific composition (ii) fast reattachment kinetics enhancing attachment and proliferation via chemical bond and (iii) controllable chemical properties^{2,3}. The prominent feature of bioactive glass is the formation of apatite like layer on their surface when they are immersed in physiological simulated body fluid (SBF)/human plasma⁴⁻⁶. The composition of this hydroxyapatite (HA) layer is almost similar to bone mineral and it provides adhesion with the surrounding tissues⁷⁻⁹.

The bioactive, mechanical and structural properties of the bioactive glasses are highly dependent upon synthesis techniques, composition, particle size and crystallization etc. Many techniques are being used to make bioactive glasses. The most common method to make a bioglass is conventional melt-quenching technique, in which all the components are mixed well using the ball mill and finally melting this mixture at high temperatures. Anyhow, the melt quenching technique may lead to volatilization of some oxides like B_2O_3 . As an alternative approach, many researchers use the sol-gel technique these days¹⁰⁻¹⁴. The bioactive glasses obtained by sol-gel technique are of high purity with increased specific surface area. In addition to this, the low synthesis temperature, high porosity, fine particle size and homogeneity of these glasses also lead to enhanced bioactivity¹⁵⁻¹⁸. However, some reports emphasized on the decreased mechanical strength of sol-gel based glasses¹⁹. Therefore, a novel composition having improved mechanical strength, cytocompatibility as well as high apatite-forming ability needs to be optimized.

Many glass compositions using copper, silver, magnesium, strontium and zinc as dopants have been studied²⁰⁻²⁸. Zinc plays an important role for skeletal system, proliferation of bone cells, enzyme regulation and DNA replication²⁹⁻³³. It is also reported that the glasses containing zinc more than 5 wt% helps in improving the

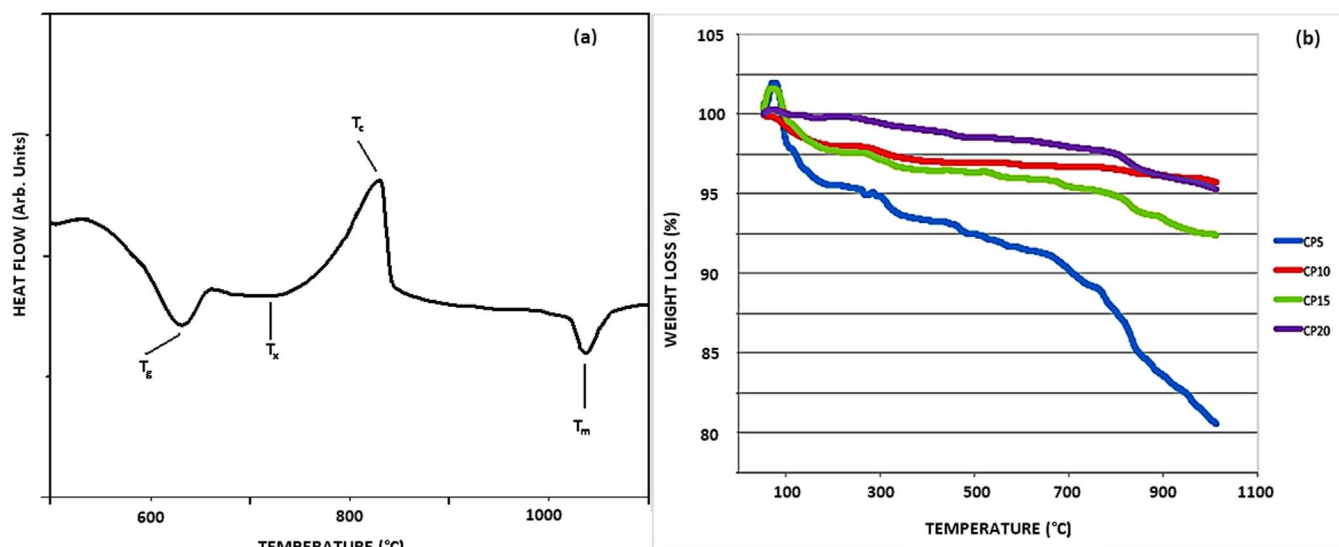


Figure 1 | (a) DSC curve for sample CP20 at heating rate of $10^\circ\text{C}/\text{min}$ and (b) Thermogravimetric analysis of all the pristine glass samples.

compressive strength and aqueous durability of glass^{34,35}. CaO , P_2O_5 and SiO_2 (CAP) are the constituent of almost all the bioactive glasses, but very few compositions have been synthesized using B_2O_3 incorporated in CAP system. Huang et al.³⁶ found substantial increase in the conversion of the glass to HA in aqueous phosphate solutions upon replacement of SiO_2 with B_2O_3 in steps. Borate/borosilicate glasses also show more controlled sintering behavior than silicate glasses^{37,38}. Hence, the focus is on the bioactive property and cytotoxicity of phosphor-borosilicate rather than phosphosilicate glass system. Saranti et al.³⁹ reported that boron exhibits catalytic effect, which enhances bioactivity. Bone implant and osteointegration using B_2O_3 based glass system is reported by Lee et al.⁴⁰ without any toxicity. Calcium plays a significant role in bioactive glasses as calcium content determines the pore size^{41,42}. The porosity affects the rate of dissolution and hence bioactivity. Hence Therefore, in present study, new novel glass composition i.e. $(25 - x)\%\text{CaO} - x\%\text{P}_2\text{O}_5 - 60\%\text{SiO}_2 - 5\%\text{B}_2\text{O}_3 - 10\%\text{ZnO}$ ($x = 5, 10, 15, 20$) has been synthesized using sol-gel method. The glasses were characterized using differential scanning calorimetry (DSC), thermogravimetric analysis (TGA), X-ray diffraction (XRD) and scanning electron microscopy (SEM). The particle size, zeta potential, and mechanical properties were also determined. Synthesized glasses were soaked in 27-Tris-SBF for different durations of 5, 15 and 30 days to assess the in-vitro apatite-forming ability using pH measurements, XRD and SEM. MTS assay cytotoxicity test were conducted on J774A.1 cells murine macrophage cells for different glass concentrations. Crystallization enhances the mechanical and flexural strength of glass due to phases embedded in amorphous glassy matrix. Therefore, the apatite-forming ability and mechanical properties of crystallized glasses have also been studied.

Results

Thermal analysis. Non-isothermal method is used to obtain various characteristic parameters from DTA. In this method, the glass sample is heated up at a fixed heating rate. The characteristic transition temperatures (T_g), onset crystallization temperature (T_x), crystallization temperatures (T_c) and melting temperatures (T_m) for pristine glasses are listed in table 2. Fig. 1 (a) shows the DSC (at a heating rate of $10^\circ\text{C}/\text{min}$) for sample CP20 indicating the characteristic temperatures. It is clear from table 2 that all the characteristic temperatures decrease with the increase in P_2O_5 content. As the melting temperature is lowest for the CP20, it implies that the increase in phosphorus content decreases the

cross-linkage inside the glass network. The weight loss is shown in fig. 1(b) respectively for all the glasses. Interestingly the weight loss is 17.93, 4.72, 8.01 and 4.81% respectively for the CP5, CP10, CP15 and CP20 glasses. CP5 shows maximum weight loss among all the samples.

X-ray diffraction. Fig. 2 and 3 (a) gives XRD of pristine sol-gel glasses and crystallized sol-gel glasses respectively. All the glasses have been heat-treated for 100 h, though the heat-treatment temperature has been chosen according to the crystallization temperature determined from DTA i.e. the sintering temperature

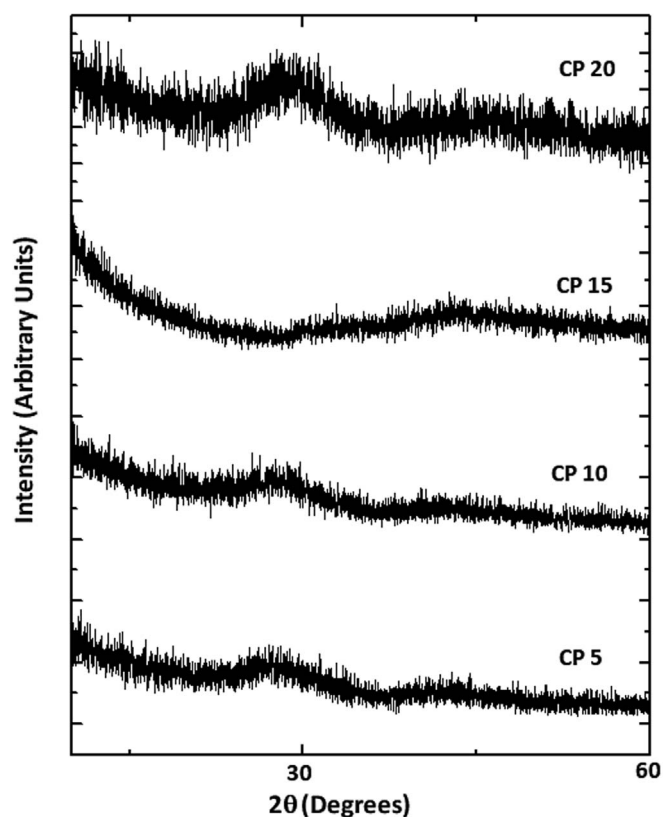


Figure 2 | XRD of pristine sol-gel glass samples.

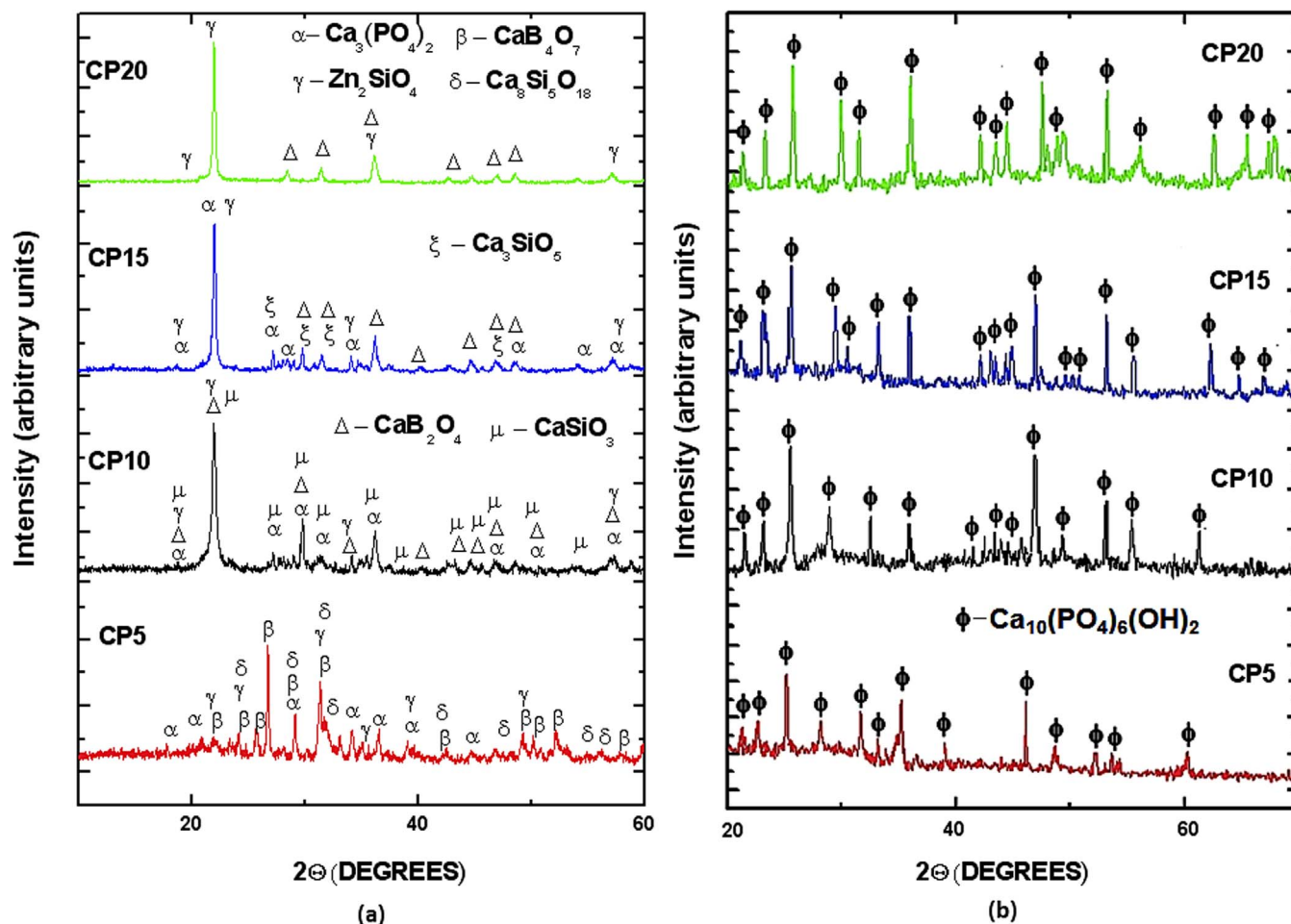


Figure 3 | (a) XRD of crystallized sol-gel glass samples after 100 h heat-treatment and (b) XRD of all the glass samples after 30 days immersion in SBF (ϕ indicates hydroxyapatite phase).

for CP5, CP10, CP15 and CP20 samples is 845, 839, 833 and 828°C respectively (table 2). Fig. 2 depicts absence of Bragg's diffraction peaks indicating the absence of crystalline phases. All the pristine glasses exhibit broad halo at low angles $\approx 27^\circ$ – 30° for the glass samples. Hence, the pristine sol-gel prepared glasses are amorphous in nature having long-range structural disorder. The diffractogram for the heat-treated sol-gel glasses (fig. 3(a)) indicate phase formation in all of them. For glass-ceramic CP5, $\text{Ca}_3(\text{PO}_4)_2$ (ICDD- 01-086-1585), Zn_2SiO_4 (ICDD- 00-001-1076), $\text{Ca}_8\text{Si}_5\text{O}_{18}$ (ICDD- 00-029-0368) and CaB_4O_7 (ICDD- 01-083-2025) phases are formed. The maximum phase fraction could be seen for CaB_4O_7 phase.

CP10 glass-ceramic exhibits CaB_2O_4 (ICDD- 01-075-0935) and CaSiO_3 (ICDD- 01-076-0186) phases along with $\text{Ca}_3(\text{PO}_4)_2$ and Zn_2SiO_4 . CP15 also exhibits same phases as that of CP10 except CaSiO_3 phase is replaced by Ca_3SiO_5 (ICDD-00-013-0209). No calcium phosphate or calcium silicate phase is seen in CP20.

Fig. 3(b) gives the XRD of all the glass samples after soaking them in SBF for 30 days. The XRD indicates the formation of hydroxyapatite on all the samples (ICDD-009-0432). This is in accordance with SEM results (discussed later on).

Particle size, zeta potential, hardness and density. The particle size, density, hardness and flexural strength of glass/glass-ceramics are obtained for all the composites are listed in table 3. Zeta potential for all the pristine glass samples after soaking in SBF is shown in fig. 4. The error bars represent standard deviation from the mean of 20 values. Particles having zeta potential between +30 mV to

–30 mV have tendency to come together⁴³. But for the particles with higher zeta potential, the repulsion between them is more and hence no flocculation or segregation of the particles occur. Initially all the sol-gel glasses possess positive zeta potential. With the increase in soaking duration, the potential becomes negative from positive. After almost 288 h of immersion in the SBF (fig. 4), both CP15 and CP20 give negative zeta potential and remained to be negative up to the end of soaking duration. In contrast to this, the zeta potential becomes negative from positive after 588 h of soaking duration for the CP5 and CP10. The density of all the pristine sol-gel glasses decreases from 2.92 to 2.76 g cm⁻³ with the increase in phosphorous content from 5% to 20% samples. Same behavior is followed by glass ceramics i.e. the density decreases from 3.12 – 2.97 g cm⁻³.

Hardness (H) and flexural strength (σ) have been calculated using following relations⁴⁴:

$$H = 1.854(P/d^2) \quad (1)$$

$$\sigma = (3 P_f L)/(2bh^2) \quad (2)$$

Where P is the applied load (Newton), d is the diagonal length (in metres), P_f is the load at which the specimen fractures, L is the length of specimen over which load is applied and h is the height of specimen. The hardness and flexural strength are listed in table 3 for pristine and crystallized glass samples.

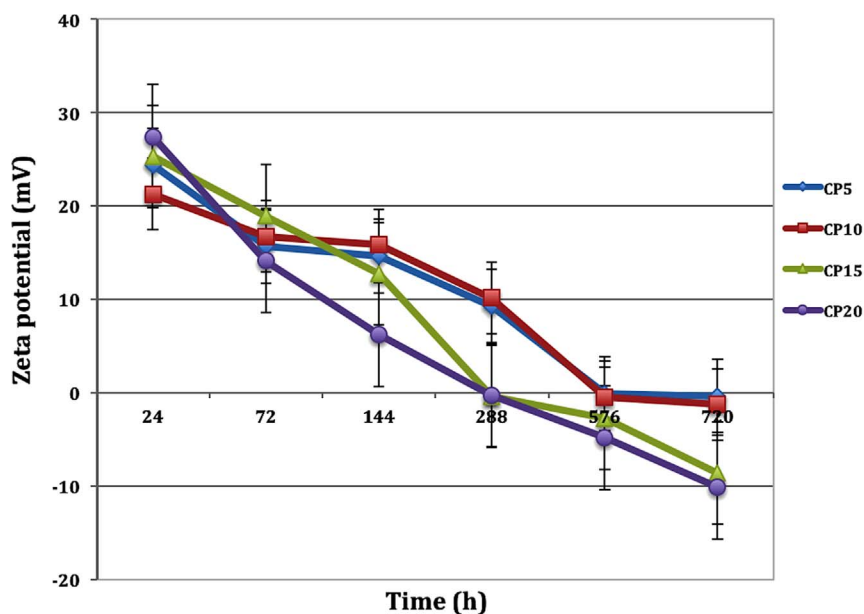


Figure 4 | Zeta potential variation of glass samples with soaking duration in SBF.

In-vitro assays in SBF solution. The pH measurements were done on the SBF solution in which glasses/glass-ceramics were soaked in order to check out their hydrolytical stability. The bioglasses usually degrade which is accompanied by dissolution of soluble species and ions depending upon the glass composition⁴⁵. The samples were immersed for 30 days. The data obtained from the pH measurement of glass/glass-ceramic soaked SBF at different time durations has been presented in fig. 5 (a–b) respectively. For both the glass and glass-ceramic, pH has shown noticeable increase as the soaking duration increases. The pH rises from 7.4 to 9.02, 7.42 to 8.95, 7.4 to 8.78 and 7.4 to 8.76 for the CP20, CP15, CP10 and CP5 glasses respectively after 720 h of soaking. For glass-ceramics also, similar trend is observed i.e. the pH rises from 7.41 to 7.99, 7.4 to 7.98, 7.42 to 8.03 and 7.4 to 8.16 for the CP20, CP15, CP10 and CP5

samples respectively after 720 h of soaking. The CP20 glass/glass-ceramic has shown highest increase in pH among all the samples.

The glass/glass-ceramics were soaked in SBF solution for 5, 15 and 30 days. Then the samples were filtered out and the morphological studies were performed using ESEM to investigate the hydroxyapatite formation on their surface. The surface morphology for all the samples is shown in fig. 6–9. As the phosphorous content increases, the layer formation also increases for both glass and glass-ceramic. Moreover, the soaking duration also directly influences the layer formation on glass/glass-ceramic surface. Though the glass-ceramics have increased strength but they show comparatively less layer formation than the pristine glasses after dipping in SBF solution. The XRD analysis of glass-ceramics also shows (fig. 3(a)), the formation of crystalline phases, which may be responsible for the higher

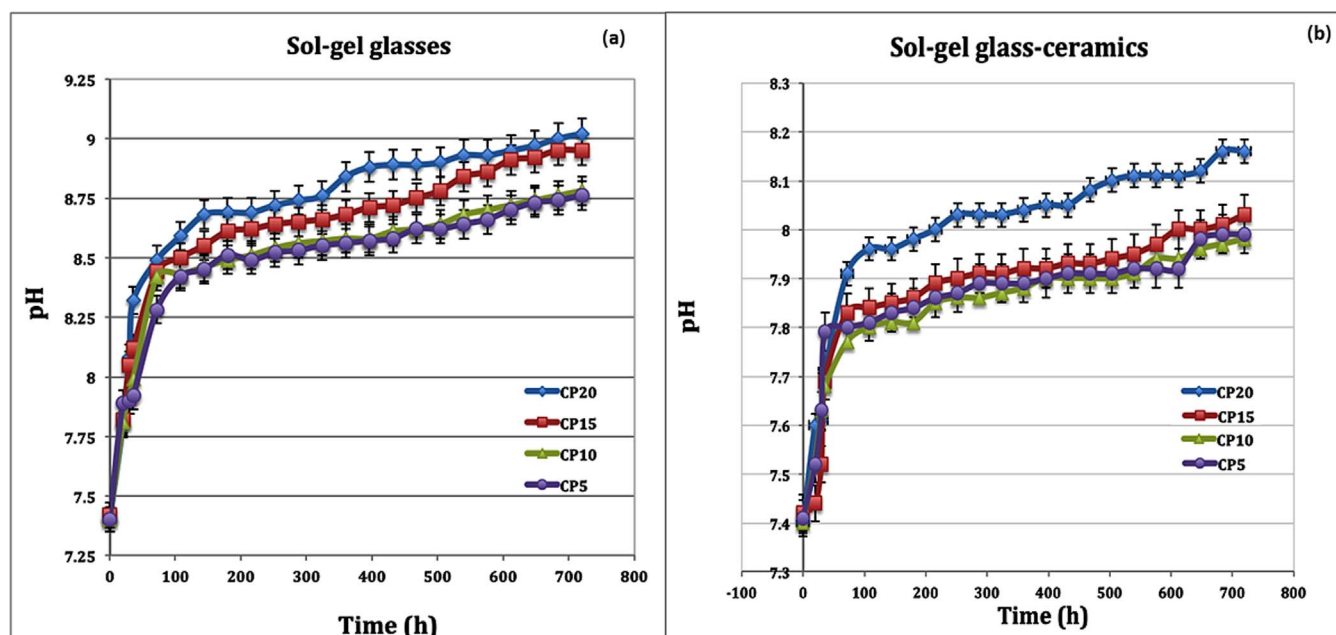


Figure 5 | (a) pH variation of pristine glasses with soaking duration and (b) pH variation of crystallised glasses with soaking duration.

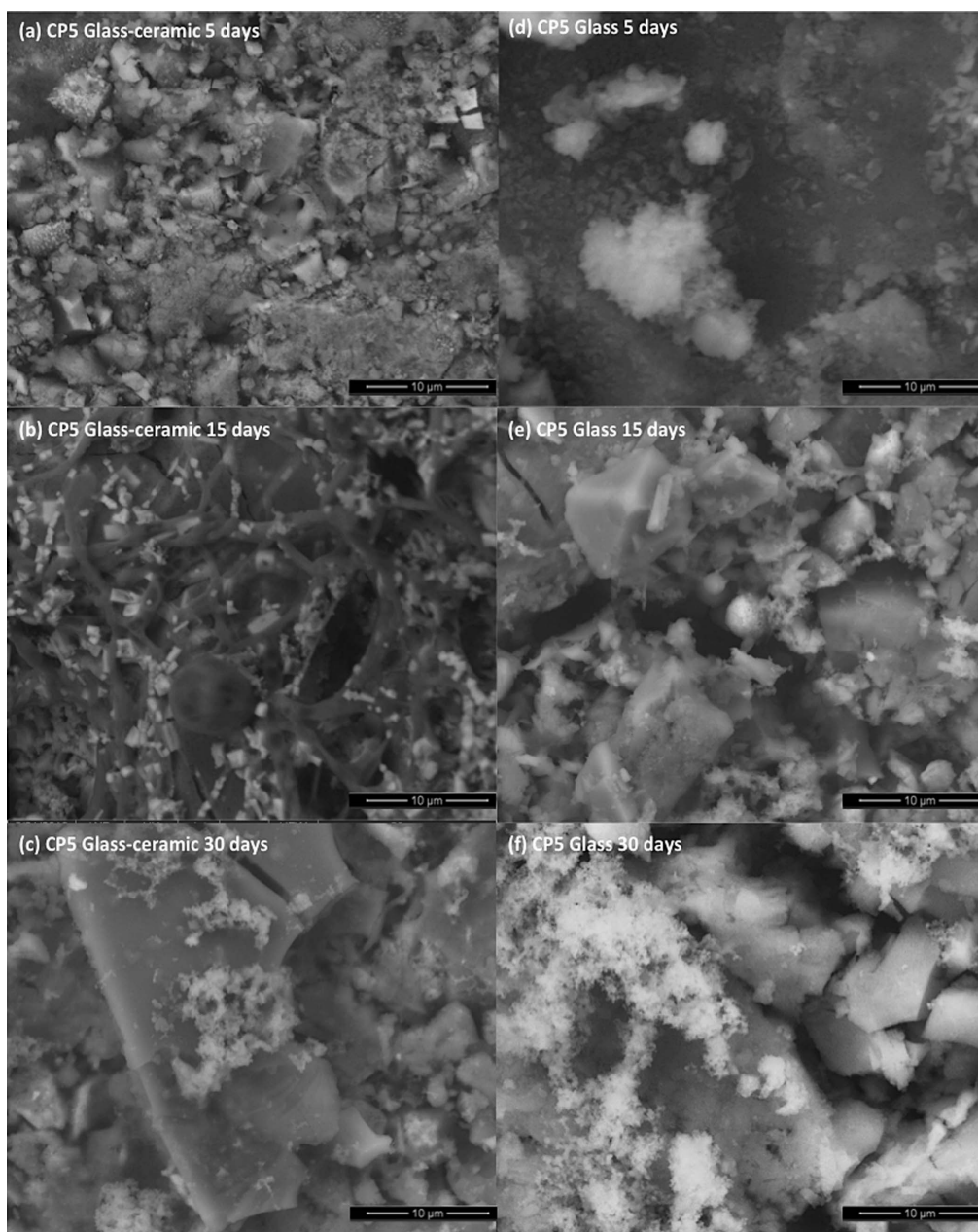


Figure 6 | Apatite layer formation for (a) 5 (b) 15 and (c) 30 days SBF soaked CP5 glass-ceramics: Apatite layer formation for (d) 5 (e) 15 and (f) 30 days SBF soaked CP5 glass.

strength of glass-ceramics and hence reduced bioactive behavior. Fig. 3(b) shows the XRD of 30 days SBF soaked samples, indicating the formation of hydroxyapatite layer on their surface. Fig. 6(a–c) shows the SEM micrograph for CP5 glass-ceramic after immersion in the SBF for 5, 15 and 30 days respectively. Fig. 6 (d–f) gives the surface morphology of pristine glasses corresponding to soaking of 5, 15 and 30 days. CP5 glass-ceramic after 5 days soaking apparently shows almost no layer formation on its surface whereas CP5 glass do exhibit some flake formation on its surface. This could be due to the fact that maximum crystalline phases are observed for this glass, which increases the mechanical integrity of the glass making the network stronger. Moreover, the pH values are also very small for CP5 glass-ceramic, which further indicates its low dissolution rate. After 15 days immersion in the SBF, CP5 glass-ceramic exhibit the formation of some flake shaped particle on its surface. These flakes have also increased after 30 days soaking. The CP5 glass is also following similar trend, where the tiny crystalline particle

concentration has increased on the surface with the increase in soaking duration from 5 to 30 days.

Figure 7 (a–c) shows the morphologies of CP10 glass-ceramic after soaking time of 5, 15 and 30 days. The surface of CP10 glass-ceramic shows crystallinity but almost smooth surface. But after soaking duration of 10 days, there is observable change in surface morphology. Acicular lath-shaped particles are observed partially covering the surface of the CP10 glass-ceramic. Furthermore, the density of these particles increased with the soaking duration of 30 days. For CP10 glass (fig. 7 (d–f)), the particles agglomerated with relative high density than the corresponding glass-ceramic. After 30 days soaking, the apatite layer has grown more and the particles are more spherical in nature. The apatite-forming ability of CP15 glass-ceramic is shown in fig. 8 (a–c), which indicates some nodules formation on the glass after 5 day soaking. The particles could also be seen on the surface of CP15 glass (fig. 8(d)) after 5 day soaking, though it is not completely covering the glass-surface. As the time duration of soak-

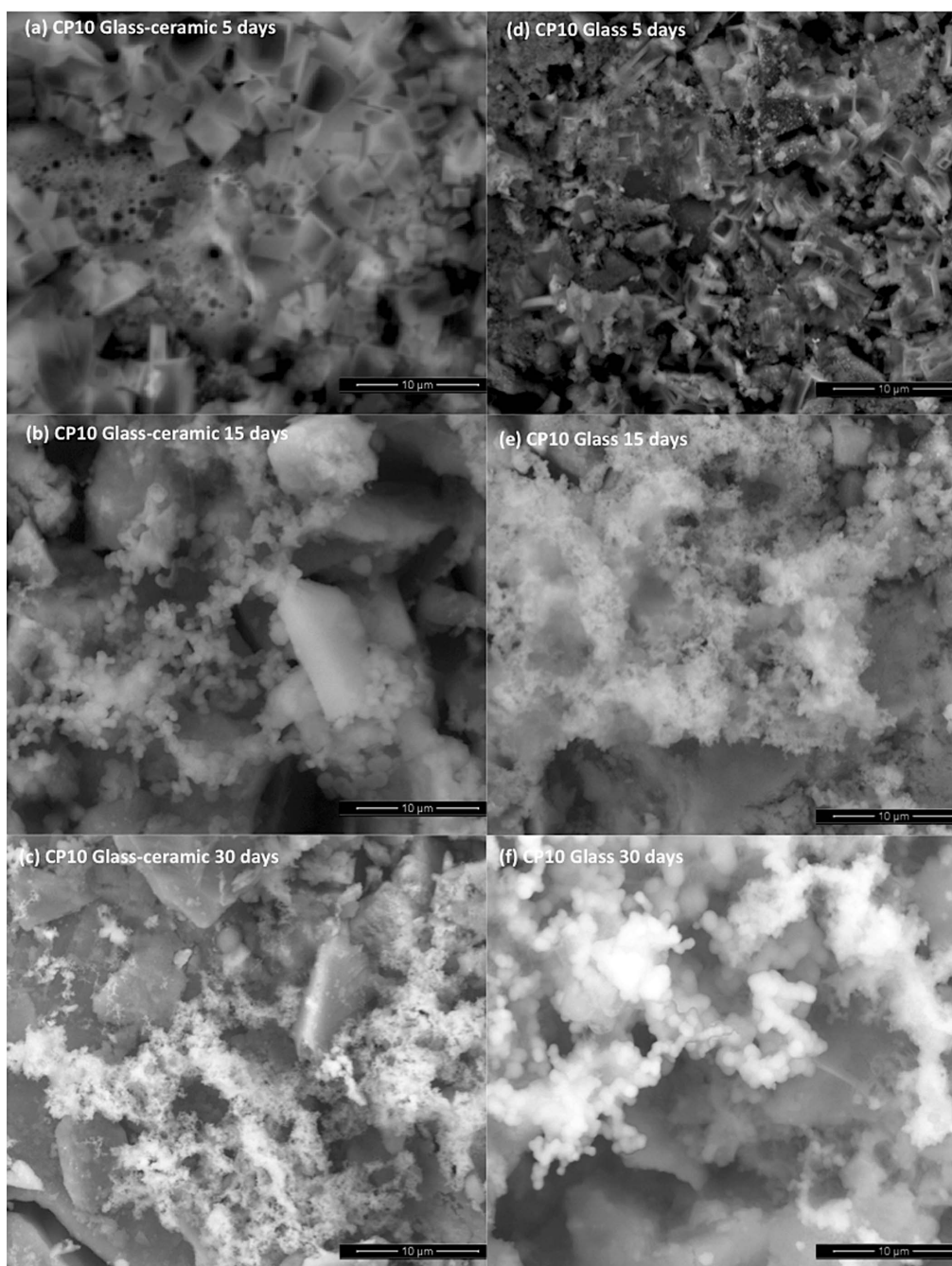


Figure 7 | Apatite layer formation for (a) 5 (b) 15 and (c) 30 days SBF soaked CP10 glass- ceramics: Apatite layer formation for (d) 5 (e) 15 and (f) 30 days SBF soaked CP10 glass.

ing increased (fig. 8 (a–f)), both CP15 glass/glass-ceramic exhibit higher layer formation and hence high apatite-forming ability. For CP15 glass, the surface is almost covered with apatite layer after 30 days of soaking (fig. 8(f)) indicating its good bioactive response.

For CP20 glass/glass-ceramic (fig. 9(a–f)), considerable HA layer could be seen on the surface after different soaking duration. The nodules combined to form big agglomerates, which finally covered the glass/glass-ceramic surface. For CP20, the maximum pH of 9.02 is obtained after 30 d of immersion in SBF implying that the CP20 should have better apatite-forming ability as compared to other samples. This is in correlation with the SEM analysis.

Cytotoxicity and MTS assays. Figure 10 shows the cytotoxicity assay for different concentration of all sol-gel glasses for the murine cells

culture. MTS assay is calorimetric assay for determining cell viability and cellular proliferation after the addition of test materials rather than toxicity. The MTS assay measures mitochondrial activity basically. It can be used to determine the TD50, i.e., when 50% of the cells are killed, which gives the most accurate values that can be reproduced similar to lethal dose 50. To make sure that the material does not kill cells, as well as replicate normally like control cells do without addition of bioglass/glass-ceramic, survival of 90 to 100% cells after exposure to a certain quantity of test material is used compared to control cells without any test material to show that it is basically not affecting the cell viability as well as cellular proliferation. Hence, in present investigation, the protocol has been modified to look at cell proliferation and survival instead of lethal dose. Therefore, the control is taken to be 100% and anything

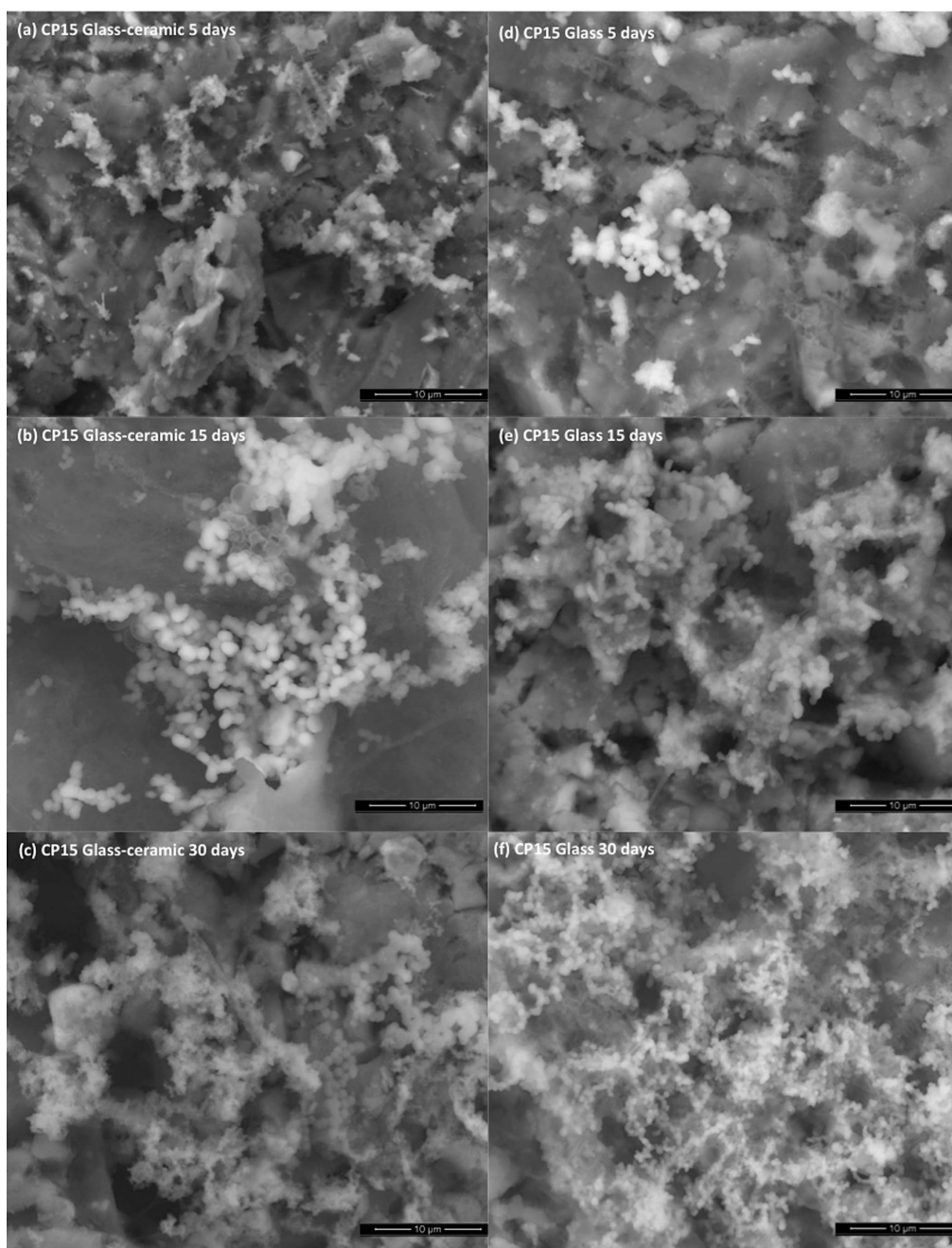


Figure 8 | Apatite layer formation for (a) 5 (b) 15 and (c) 30 days SBF soaked CP15 glass- ceramics: Apatite layer formation for (d) 5 (e) 15 and (f) 30 days SBF soaked CP15 glass.

below 90% is considered to be toxic⁴⁶. Usually, cytotoxicity is associated with reactivity of compounds. If the ionic exchange is more between glass particles and the environment⁴⁷, then the surface modifications lead to sample higher cytotoxicity. Starting from the concentration of 500 to 0.97 µg/mL, upto 15.62 µg/mL of concentration all the pristine glass samples are toxic (fig. 10). At 7.81 µg/mL of concentration, glass sample CP5 and CP15 still showed some toxicity whereas sample CP10 and CP20 are not in the acceptable regime. When the concentration of sol-gel glass is further reduced to 1.95 µg/mL, then all the glasses except CP20 are non-toxic. Furthermore, all the samples are non-toxic at a concentration of 0.97 µg/mL. Fig. 11(a) demonstrates the MTS plates of all sol-gel glasses at different concentrations. The cytotoxicity assay of glass-ceramics at different concentration is shown in figure 11(b). From fig. 11(b), it is clear that glass-ceramic

CP20 is non-toxic even at 500 µg/mL, though all other glasses are toxic at that concentration. At all the other concentrations, cell viability is high and almost equal or above the control level. The results for live-dead cell assay results for all glasses at three concentrations of 7.81, 1.95 and 0.97 µg/mL are shown in fig. 12. Only those compositions are chosen which show maximum cell viability in MTS assay. The average control level of live cell viability is 81.5% and that of dead cell is 18.5%. Figure 13 gives the live-dead viability results for crystallized glass-ceramics. For analyzing the live-dead cell assay of glass-ceramics, the concentrations were chosen to be 500, 250 and 125 µg/mL which are different from the one taken during analysis of pristine glasses. These concentrations are chosen because almost all the concentrations show non-toxicity except 500 µg/mL. The average live cell control level is 96% and rest 4% is control level of the dead cells.

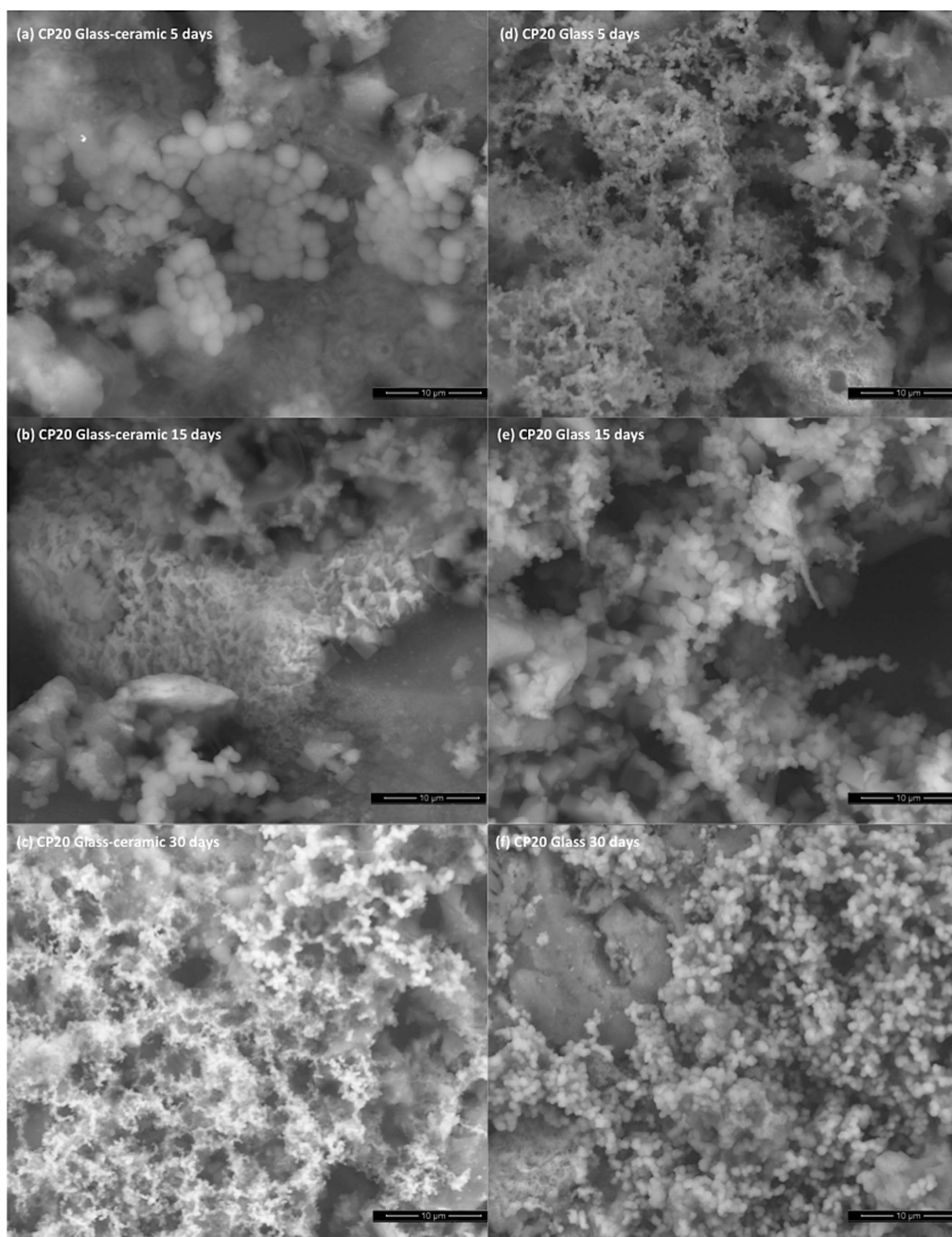
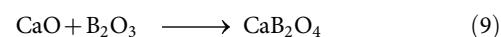
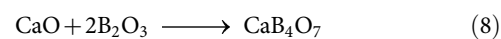
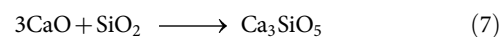
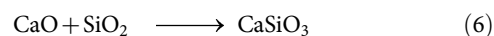
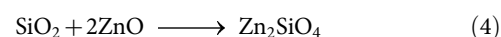
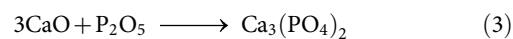


Figure 9 | Apatite layer formation for (a) 5 (b) 15 and (c) 30 days SBF soaked CP20 glass- ceramics: Apatite layer formation for (d) 5 (e) 15 and (f) 30 days SBF soaked CP20 glass.

Discussion

The weight loss is attributed to the evaporation of water, volatility of organic components and loss of the hydroxide (OH) groups⁴⁸. The precursors used for the glass synthesis are mainly nitrates, and the main weight loss occurs between 200–600°C, which is due to nitrate decomposition and condensation by-products. All other glasses show weight loss less than 10%. Generally sol-gel prepared glasses show high weight loss i.e. between 30–40%. But the present glasses do not exhibit such kind of weight loss behavior. The main reason for this behavior can be the higher calcination time of 12 h, which already made the glass free from nitrate products. Hence, the glasses exhibit quite stable thermal behavior in terms of weight loss. It is clear from fig. 3(a) that the CP5 glass-ceramic exhibits maximum crystallization. The crystallization and hence phase fraction decreases with increase of phosphorus content in samples. The various reactions, which might have taken place, are proposed as follows:





MTS Cytotoxicity Assay for Sol-Gel Glasses

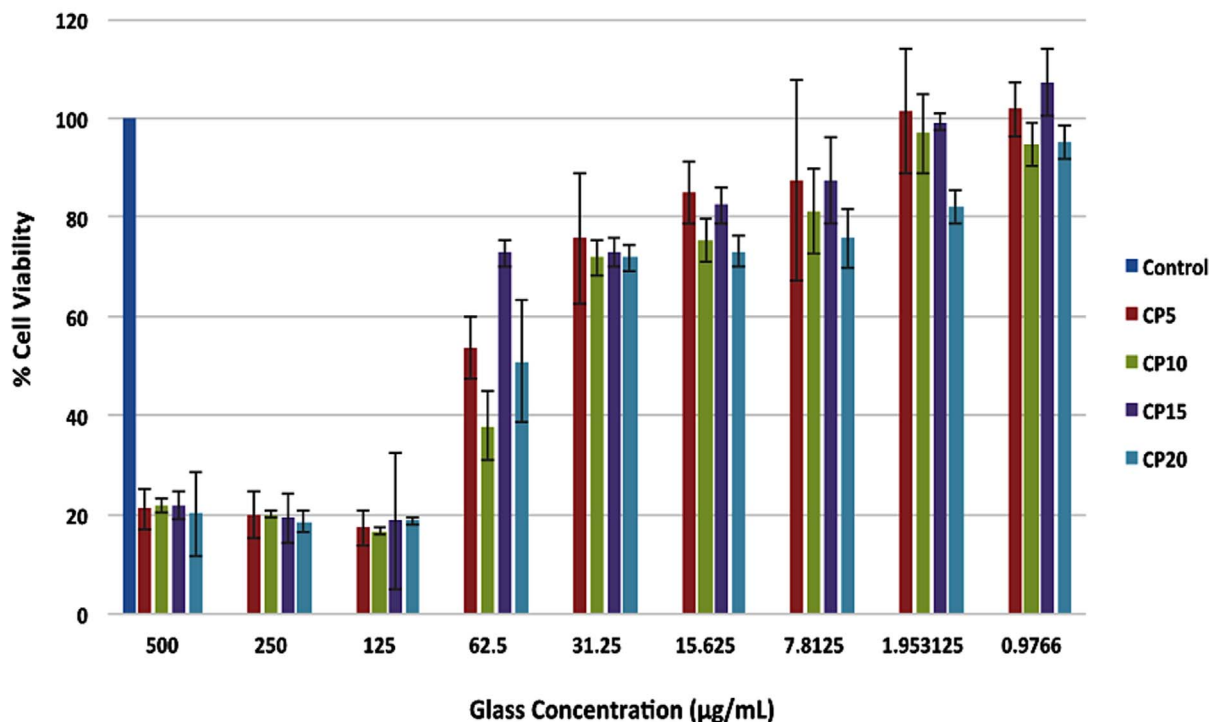
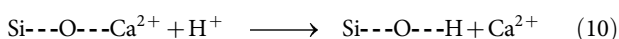


Figure 10 | MTS cytotoxicity assay results for pristine glasses at different concentrations for murine cells culture.

$\text{Ca}_3(\text{PO}_4)_2$ is also known as whitlockite phase and is component of tooth enamel and bone mineral⁴⁹. It is absent in CP20 glass-ceramics inspite of fact that it has high amount of phosphorus. Boron, phosphorus and silicon have interacted with network modifiers calcium oxide and zinc oxide via non-bridging oxygens. In CP5 glass-ceramic, calcium is having highest content among all the other samples, which means more non-bridging oxygens. Hence, Si^{4+} , B^{3+} and P^{5+} have bonded with Ca^{2+} via non-bridging oxygens. But at 5% concentration of CaO, phosphorus does not do any bonding with calcium.

The potential, which exists between the dispersing liquid and particle surface and varies according to the distance from particle surface is called zeta potential. Generally zeta potential gives a direct measure of inter-particle repulsive force and the flocculation tendency of particles^{50,51}. The behavior of zeta potential as depicted from fig. 4 can be explained as follows^{52,53}:

- (1) Upon soaking in SBF, the silanol (Si-OH) groups are formed due to the exchange of ions between the H^+ from the solution and the glass network modifier Ca^{2+} and hence hydrolysis of the silica groups occurs. The reaction mechanism follows the equation:



During the initial duration of the soaking, the release of ion may counterbalance each other, hence making zeta potential neutral. Particularly, in CP5 and CP10 sol-gel glass, the calcium extent is higher, hence more of the Ca^{2+} ion can combine with OH^- making the solution positive.

- (2) As the phosphorus content increases from 5% to 20%, the HPO_4^{2-} content increases in solution. Hence, HPO_4^{2-} may incorporate into the bulk and PO_4^{3-} migrates from bulk towards the glass surface, which makes the surface negative. Hence, for the CP15 and CP20, the glasses show negative negative zeta potential quite early in comparison to CP5 and CP10.

In-vivo, the negative zeta potential promote cell proliferation and attachment⁵⁴. The CP20 gives the lowest particle size and CP10 gives the highest size. The change of glass to glass ceramics due to devitrification upon heat-treatment resulted in increase of density as is evident from table 3. The high density of the CP5 glass/glass-ceramics indicates its high cross-linking density in its network. In addition to this, the hardness as well as flexural strength decreases from sample CP5 to CP20 with increase in phosphorus content (table 3). This is in accordance with the variation of density for all glasses. This trend is attributed to the replacement of heavier calcium oxide (3.35 g cm^{-3}) with lighter phosphorus oxide (2.39 g cm^{-3}). Both the hardness and flexural strength are obtained to be highest for crystallized samples than the amorphous pristine glasses as is clear from table 3. The crystallization process also lead to mitigation of glass so as to fill the gaps or pores, which subsequently lead to increase in density and hence mechanical properties also.

pH has shown appreciable change over period of the soaking for the glass as well as glass-ceramics (fig. 5(a–b)). This increase in pH is mainly attributed to the exchange of Ca^{2+} ions from the glass with H_3O^+ ions in the SBF solution²⁵. In other words, the leaching of ions from the glass matrix increases the concentration of silicon and calcium in the SBF and subsequent formation of calcium phosphate takes place, which decreases the concentration of the phosphorus and calcium in solution⁵⁵. Hence, prior to the hydroxyapatite formation, silica gel layer is formed on the surface of glass. From fig. 5(a), it is clear that the pH increased very rapidly after initial 100 h of immersion in SBF solution for all the pristine glass samples. pH follows the trend $\text{pH}_{\text{CP20}} > \text{pH}_{\text{CP15}} > \text{pH}_{\text{CP10}} > \text{pH}_{\text{CP5}}$. For the CP20 glass sample, the pH rises from 7.4 to 8.49 after 108 h of dipping. Similarly, for all the other samples, it rises from 7.42 to 8.44, 7.4 to 8.42 and 7.4 to 8.28 for the CP15, CP10 and CP5 respectively. After 100 h, the pH rises slowly. The maximum pH value is 9.02, which is obtained from the CP20 after 720 h of soaking. CP15 gives pH value of 8.95 followed by 8.78 and 8.76 by CP10 and CP5 respectively after 720 h of dipping in SBF.

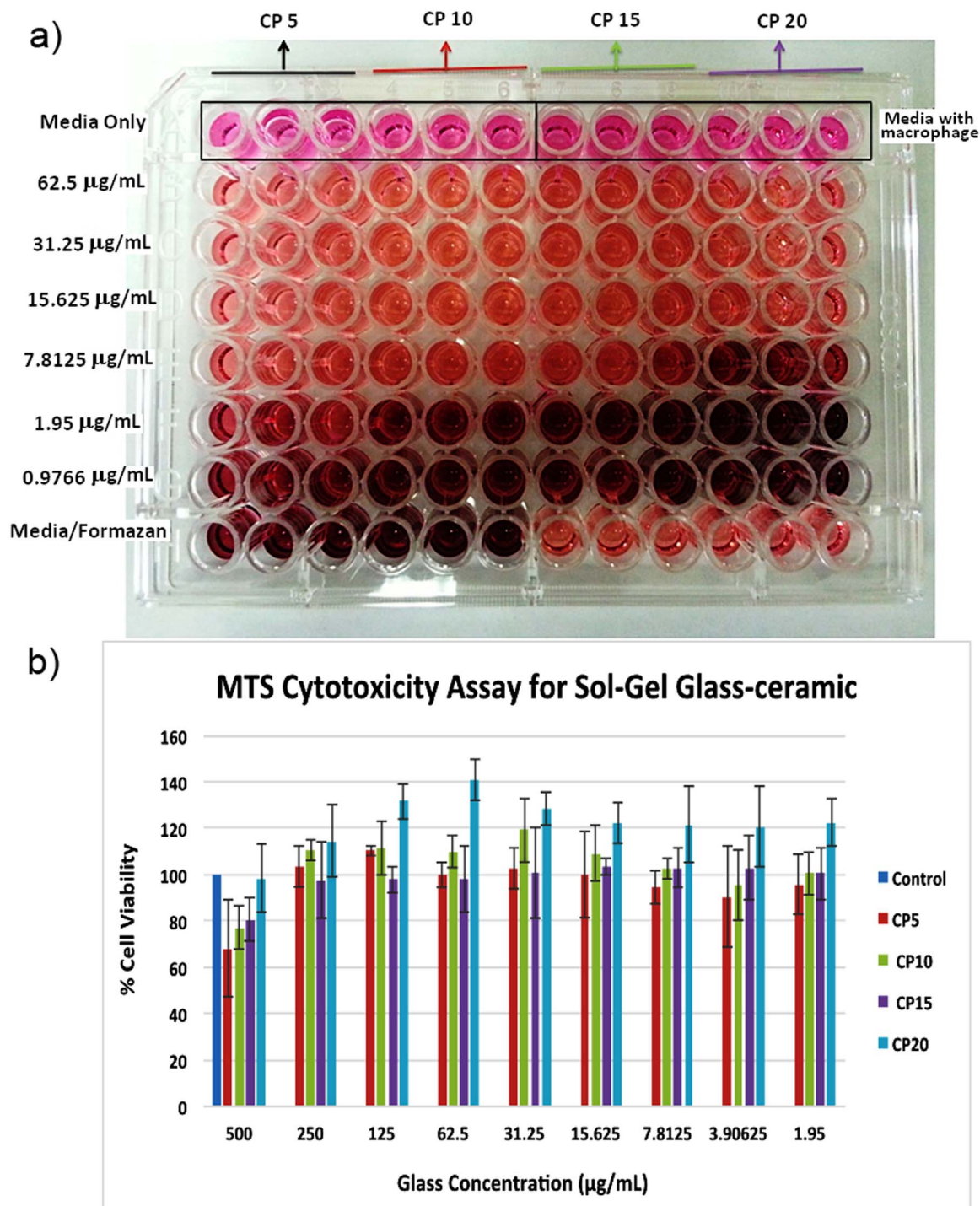


Figure 11 | (a) The plates for cytotoxicity assays of sol-gel glasses and (b) MTS cytotoxicity assay results for crystallised glasses at different concentrations for murine cells culture.

Almost similar trend is followed by the glass-ceramics also as depicted from fig. 5(b). The maximum pH is shown upto initial 70 h of soaking due to faster release of the Ca^{2+} , PO_4^{3-} , and Si^{4+} ions. But the pH values of glass-ceramics are comparatively lower than the values of pH obtained from pristine glasses after dipping. This could be attributed to the fact that the glasses are amorphous with random loose network, which allows faster exchange of the ions. In contrast to this, the crystalline phases embedded in the amorphous glassy matrix of glass ceramics increase the structural integrity hindering the migration of ions. However, the pH variation is highest for the CP20 glass-ceramic again i.e. maximum pH of 8.16 is obtained

after 720 h of immersion in SBF. Hence, increase in the phosphorus content has increased the maximum dissolution. The maximum pH values of the CP15, CP10 and CP5 glass-ceramics are quite close to each other.

Hydroxyapatite is a naturally occurring mineral as well as prominent component of tooth enamel and vertebrate bone having stoichiometry of $\text{Ca}_{10}(\text{PO}_4)_6(\text{OH})_2$ ⁵⁵. The Ca/P ratio is 1.67 and lower Ca/P ratio leads to higher solubility and acidity. Biological bone forming apatite crystals are less than 500 Å in size. They are non-stoichiometric calcium deficient and have carbonate in their structure unlike hydroxyapatites. The carbonate (CO_3^{2-}) in biological apatites

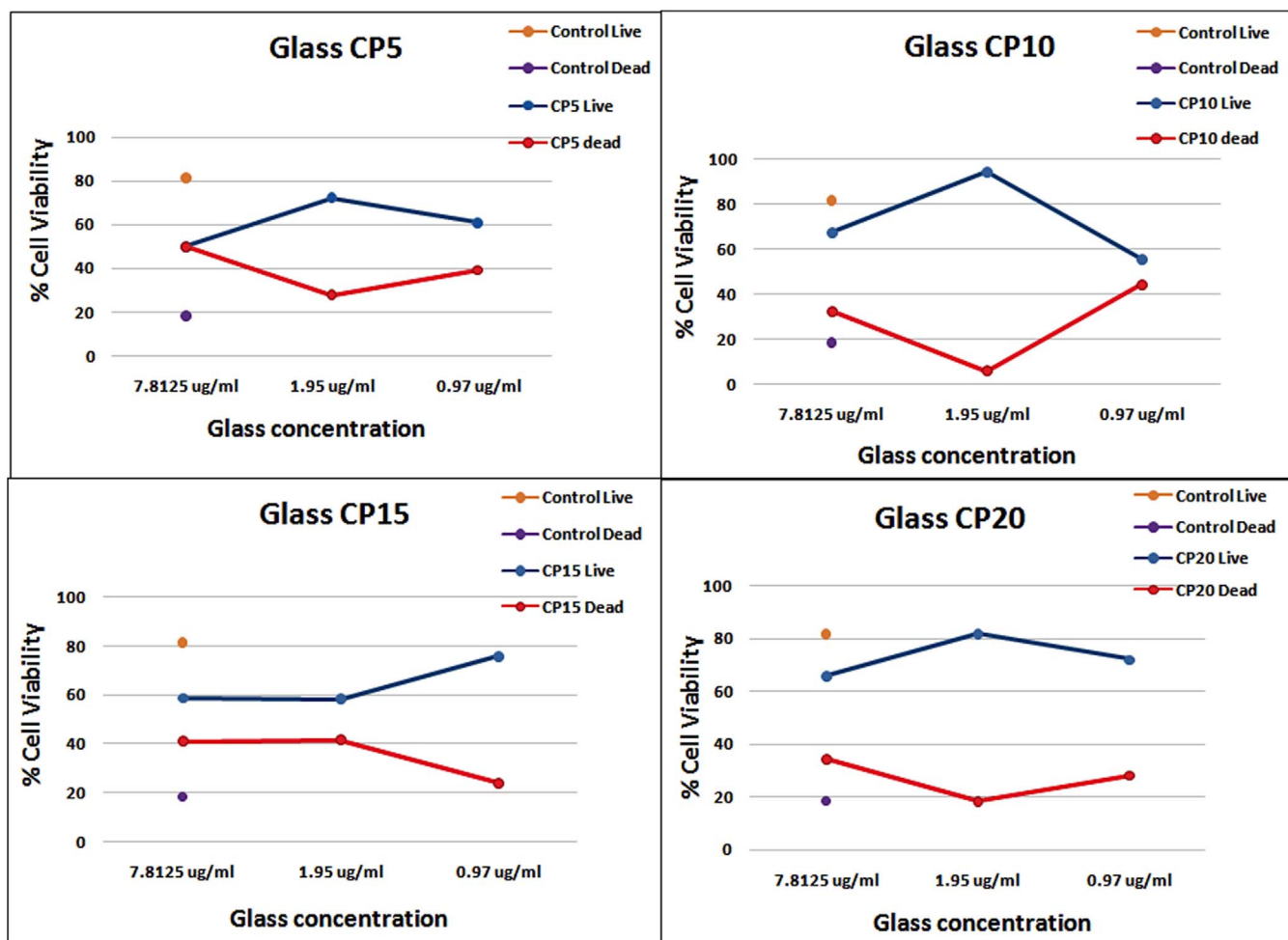


Figure 12 | Live-dead cell viability for pristine glasses at optimum concentrations.

cause stresses and lattice distortion further leading to solubility. The OH^- in hydroxyapatite can be substituted by CO_3^{2-} for synthetic non-aqueous systems i.e. dissolved CO_2 in the aqueous phosphate solution contributes to carbonate⁵⁶.

From the SEM micrograph given in fig. 6 (a–f), it is observed that CP5 glass exhibit some flake formation on its surface after 5 days of soaking whereas CP5 glass-ceramic shows almost no layer formation on its surface. The high crystallinity of CP5 glass-ceramic made the network stronger thereby decreasing the pH and hence low dissolution rate. Some flake shaped particles deposit on the surface of CP5 glass/glass-ceramic after 15 days immersion in the SBF solution. Furthermore, the density of these flakes increase with the increase in soaking duration.

The morphologies of CP10 glass-ceramic after soaking time of 5, 15 and 30 days are shown in figure 7 (a–f). The surface morphology of CP10 glass/glass-ceramic changes after dipping it in SBF for 15 days i.e. Acicular lath-shaped particles partially cover their surface. After 30 days soaking in the SBF, lath shaped particles turn more or less into spherical shape and their concentration increases on the CP10 glass/glass-ceramic surface.

Similarly, partial nodules formation could be seen on the surface of CP15 glass/glass-ceramic after 5 day soaking (fig. 8(a–f)). After 30 days of soaking, CP15 glass surface is almost covered with these nodules indicating its good bioactive response. For CP20 glass/glass-ceramic (fig. 9(a–f)), HA layer formation in form of big agglomerates could be observed on the surface after different soaking duration. The formation of HA could be confirmed from the XRD of SBF soaked samples as shown in fig. 3(b). This almost covers the

whole glass/glass-ceramic surface after 30 days immersion in SBF solution. The maximum pH of 9.02 for CP20 glass is obtained after 30 days of immersion in SBF indicating its better apatite-forming ability among other samples. Hence, SEM analysis correlates well with the pH results. Following points are obtained during micro-structural analysis:

- For all the samples, the pristine glass samples have shown higher bioactive response than the corresponding sintered sample. This clearly indicates that crystallinity hinders the apatite formation.
- With the increase in soaking duration, the apatite formation increased for all glass/glass-ceramics.
- Increase in bioactive behavior has been observed with decrease in calcium content/increase in phosphate content i.e. CP20 glass/glass-ceramic exhibits highest pH values and layer formation as compared to other samples.

From the cytotoxicity results (fig. 10), it is clear that, glass sample CP5 and CP15 are almost non-toxic at 7.81 $\mu\text{g}/\text{mL}$ of concentration. Except CP20, all the glasses show non-toxic behavior at concentration of 1.95 $\mu\text{g}/\text{mL}$. At a concentration of 0.97 $\mu\text{g}/\text{mL}$, all the samples exhibit non-toxic behavior. But in contrast to this, glass ceramics are non-toxic even at higher concentrations as indicated from fig. 11(b) especially glass-ceramic CP20 exhibits highest viability among all the samples. This further indicates the non-toxicity of phases formed in glass-ceramic. Furthermore, the live-dead cell assay count indicates that CP5 gives the maximum viability of 72.3% at concentration of 1.95 $\mu\text{g}/\text{mL}$ (fig. 12). Glass CP10 also gives the

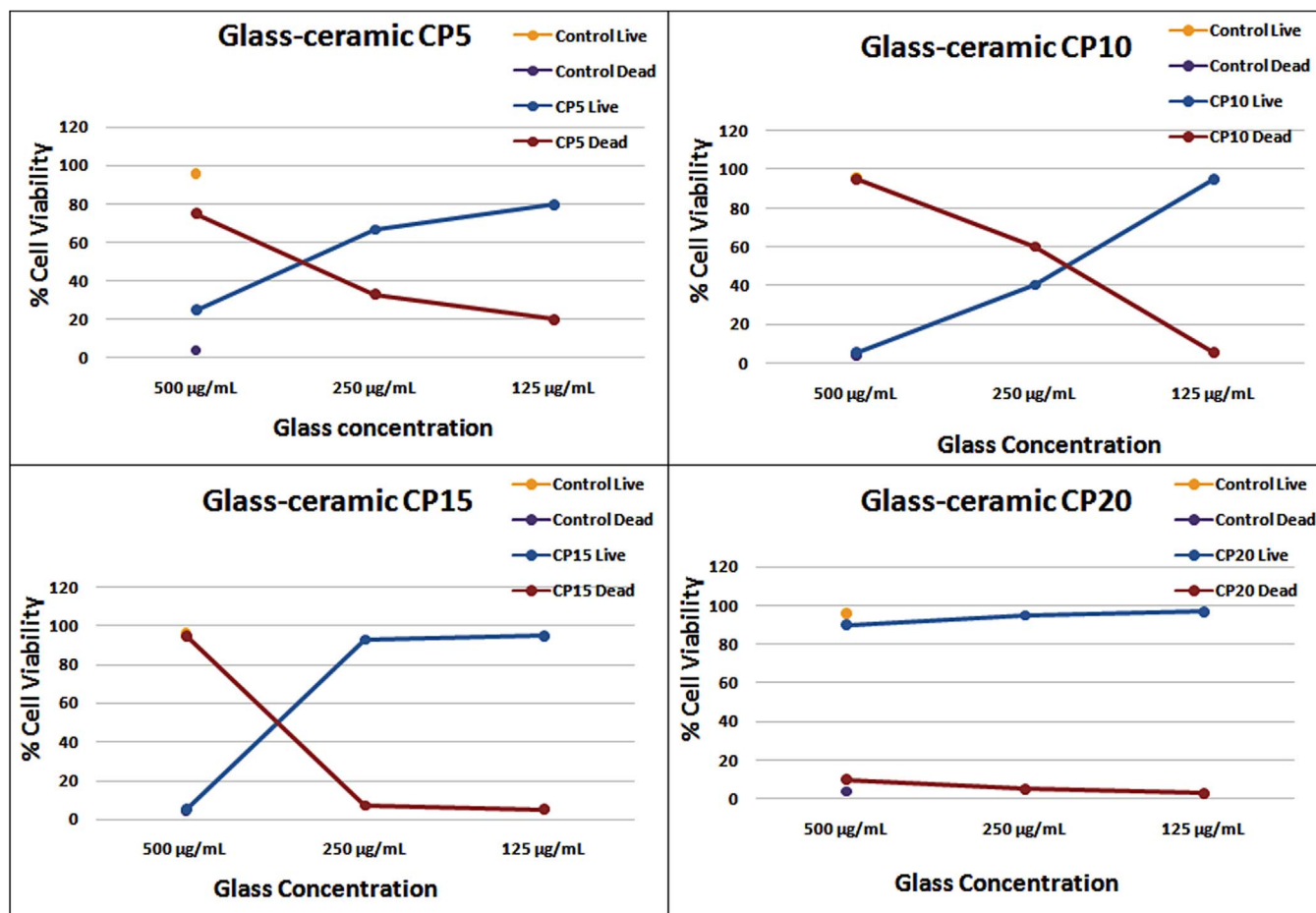


Figure 13 | Live-dead cell viability for crystallized glasses at optimum concentrations.

maximum live-cell viability of 94.2% at 1.95 µg/mL, whereas CP15 exhibits maximum viability of 75.9% at 0.97 µg/mL. Glass CP20 also gives the maximum live cell count of 81.4% at 1.95 µg/mL.

For CP5 glass-ceramic, at all the concentrations, the live cell count is below the control level (fig. 13). CP10 glass-ceramic gives live cell viability to be 95% at 125 µg/mL whereas at 500 µg/mL the viability is only 5%. Furthermore, the live cell count is almost acceptable at 250 µg/mL also in addition to 125 µg/mL concentration for CP15 glass-ceramic. But CP20 glass-ceramic gives 90% live cell viability even at 500 µg/mL. CP20 shows maximum live cell count among all the samples. These MTS assay results show that the toxicity reduces with crystallinity. At low concentrations, the pristine glasses also give cytotoxicity above control level.

Conclusively, all these glasses show weight loss less than 10% obtained from thermogravimetric analysis. CP5 glass-ceramic exhibited maximum crystallization. Furthermore, the crystallization and hence phase fraction decreased with increase of phosphorus content in samples whereas reverse trend was followed for density and hardness. The pristine glasses possess positive zeta potential. As the soaking duration increased in SBF, the potential became negative from

positive indicating their more flocculation tendency. Increase in the phosphorus content has increased the maximum dissolution as indicated from the pH measurements. The MTS assay results indicated that toxicity decreased for crystalline glasses. Glass-ceramic CP20 shows the highest viability among all the crystallized samples. The microstructural studies also indicate increase in hydroxyapatite layer formation on the surface of glass/glass-ceramic with the soaking duration as well as increase in phosphorus content. Though crystallization has enhanced mechanical properties, density and reduced the toxic effects, but it has decreased the apatite layer formation due to lower dissolution rate of ions. Glass-ceramics could be used at higher concentration as revealed by live-dead cell assay. Conclusively, CP20 glass/glass-ceramic possesses highest apatite-forming ability and less toxicity among all other samples. It can be further investigated as potential material for bone regeneration.

Methods

Sol-gel synthesis. The glass composition $(25 - x)\%CaO - x\%P_2O_5 - 60\%SiO_2 - 5\%B_2O_3 - 10\%ZnO$ ($x = 5, 10, 15, 20$) was synthesized using the sol-gel technique. The glass compositions along with their sample labels are given in table 1. The glass CP5

Table 1 | The compositions of sol-gel glasses along with sample label (mol %)

Sample	CaO	P ₂ O ₅	B ₂ O ₃	SiO ₂	ZnO
CP5	20	5	5	60	10
CP10	15	10	5	60	10
CP15	10	15	5	60	10
CP20	5	20	5	60	10

Table 2 | Characteristic temperatures obtained by DSC for all the glasses

Sample	T _g	T _x	T _c	T _m
CP5	659	730	845	1060
CP10	642	724	839	1044
CP15	638	718	833	1032
CP20	633	716	828	1022



Table 3 | The particle size, density, hardness and flexural strength for all glass/glass-ceramic samples

Sample	Particle size (nm)	Density (g cm ⁻³)		Hardness (GPa)		Flexural strength (MPa)	
		Glass	Glass ceramic	Glass	Glass ceramic	Glass	Glass-ceramic
CP5	320.71	2.92	3.12	4.83	87.52	7.33	113.28
CP10	412.16	2.87	3.08	4.72	79.81	7.01	109.72
CP15	389.92	2.81	3.01	4.54	72.33	6.83	103.41
CP20	312.59	2.76	2.97	4.42	59.12	6.42	91.22

was prepared by hydrolysis and polycondensation of 20.722 mL of tetraethyl orthosilicate (TEOS), 2.64 mL of triethyl phosphate (TEP), 7.33 g of calcium nitrate tetrahydrate, 4.62 g of zinc nitrate hexahydrate and 0.48 g of boric acid. The TEOS and TEP hydrolysis was catalyzed using 1 M HNO₃ and the molar ration was kept to be HNO₃ + deionized water: TEOS + TEP = 8: 1. The reactants were added consecutively after every 0.5 h of continuous stirring. The sol was kept in the sealed polyethylene containers at the room temperature and was allowed to gel. The dried gel was then ball-milled for 3 h to obtain homogenous particles and then stabilized at 600°C for 12 h. The powders were again ground and pelletized in hydraulic press under 200 MPa to make compact discs of 10 mm × 3 mm. The compact samples were sintered in high temperature furnace with a heating rate of 5°C/min at a suitable temperature determined from DTA and TGA. The density of glass/glass-ceramics was calculated using Archimedes method (i.e. immersion in diethyl phthalate).

Characterization. The glass transition temperature (T_g), onset crystallization temperature (T_x), crystallization temperatures (T_c) and melting temperatures (T_m) was obtained using the differential scanning calorimetry (DSC) at a heating rate of 5°C/min. The DSC and weight loss measurements were carried out in the Netzsch 402 EP using alumina as the reference material and in an air atmosphere. The amorphous pristine glass and crystallized heat-treated glass were analyzed using high-resolution XRD in an X'Pert PRO diffractometer (PANalytical B.V., EA Almelo, The Netherlands). The particle size and zeta potential of the prepared (unsintered) samples were determined using dynamic light scattering (DLS) based Zetasizer nano series. The sample of concentration 0.1 g l⁻¹ was prepared using the methanol as a reference solution. 633 nm laser light was used to illuminate the particles within the sample at a scattering angle of 17 degrees. Cumulative method and polydispersity index were used to determine the diameter. LECO LM247AT Microhardness Tester and Control Software are used for measuring micro hardness of the samples. Flexural strength is obtained from the Q-series universal testing machine (ESM 301). The samples were polished well before the hardness and flexural measurements. Scanning electron measurements were carried out using the environmental ESEM (FEI Quanta 600 FEG, Hillsboro) with ET detector and low pressure of 1 Torr under hydrated conditions.

Cytotoxicity and MTS assay. J774A.1 cells (murine macrophage cell line from American Type Culture Collection) cells were routinely grown as monolayers in 75 cm² tissue culture flasks (Corning, Inc.) in a humidified incubator with 5% CO₂ atmosphere at 37°C. The cells were maintained in the Dulbecco's modified Eagle's medium (Sigma-Aldrich) supplemented with 10% fetal bovine serum (FBS), L-glutamine, NaHCO₃, pyridoxine-HCl, and 45,000 mg/L glucose and preserved with 1% penicillin-streptomycin solution (Mediatech, Inc.). Cultured J774A.1 cells were gently scraped at 80–90% confluency in 10 mL of culture media 10% FBS. Each sample was pipetted in 9 wells of a 96 well plate in triplicate at desired concentrations, including untreated control samples as given below to a total volume of 200 µl. The cells were incubated overnight at 37°C and 5% CO₂. 20 µL of CellTiter 96® Aqueous reagent solution was then pipetted into each well, except no formazan control wells and media only wells and then the plates were incubated for 1–4 hours at 37°C in a humidified 5% CO₂ atmosphere. The absorbance at 490 nm was recorded using a 96-well Elisa plate reader in triplicate. Statistics on data include the two-tailed T test. To make the MTS solution, 100 µL of dye into 2 mL of MTS solution was used. The cells were exposed to all the samples, at the nanoparticle concentrations of 500, 250, 125, 62.5, 31.25, 15.625, 7.8125, 3.90625, and 1.95 µg/ml for 24 hours before adding the MTS assay solution and then incubated for 1–4 hours before taking a reading. Trypan blue exclusion assay was used for live-dead cell counts. For trypan blue staining, 500 µL of cells were incubated for 3 min at room temperature with an equal volume of 0.4% (w/v) trypan blue solution prepared in 0.81% NaCl and 0.06% (w/v) dibasic potassium phosphate. Cells were counted in their respective chamber in the 4 chamber culture slide (BD Falcon CultureSlides) and a light microscope. One hundred viable and nonviable cells were recorded separately to figure out a percentage of live and dead cell counts.

In-vitro assays in SBF solution. The SBF solution was prepared using the required ion concentrations⁵⁷. The glass/glass-ceramics pellets were dipped in SBF solution kept in clean glass bottles. The bottles were tightly covered and kept in water bath at 37°C. The pH and zeta potential was measured regularly after continuous interval of dipping. The pH was measured using Mettler-Toledo pH meter (TMP-85). After the soaking process, the samples were washed with deionized water. The apatite layer formation was studied under environmental SEM and XRD.

- Hench, L. L., Splinter, R. J., Allen, W. C. & Greenlee, T. K. Bonding mechanisms at the interface of ceramic prosthetic materials. *J. Biomed. Mater. Res.* **2**, 117–141 (1972).
- Hench, L. L. & Anderson, O. H. *Advanced series in ceramics* (Eds: Hench, L. L. & Wilson, J.), Scientific Publishing Co., Singapore 1993.
- Erol, M., Ozyuguran, A. & Celebican, O. Synthesis, Characterization, and In Vitro Bioactivity of Sol-Gel-Derived Zn, Mg, and Zn-Mg Co-Doped Bioactive Glasses. *Chem. Eng. Technol.* **33**, 1066–1074 (2010).
- Hench, L. L. & West, J. K. Biological applications of bioactive glasses. *Life Chem. Rep.* **13**, 187–241 (1996).
- Hench, L. L. Bioceramics: from concept to clinic. *J. Am. Ceram. Soc.* **74**, 1487–1510 (1991).
- Bohner, M. & Lemaître, J. Can bioactivity be tested in vitro with SBF solution? *Biomaterials* **30**, 2175–2179 (2009).
- Ducheyne, P. Bioceramics: materials characteristics versus in vivo behavior. *J. Biomed. Mater. Res.* **21**(A2 Suppl.), 219–236 (1987).
- Kokubo, T. & Takadama, H. How useful is SBF in predicting in vivo bone bioactivity? *Biomaterials* **27**, 2907–2915 (2006).
- Kokubo, T., Kushitani, H., Sakka, S., Kitsugi, T. & Yamamuro, T. Solutions able to reproduce in vivo surface-structure changes in bioactive glass-ceramic A-W. *J. Biomed. Mater. Res.* **24**, 721–734 (1990).
- Balamurugan, A. *et al.* Development and in vitro characterization of sol-gel derived CaO–P₂O₅–SiO₂–ZnO bioglass. *Acta Biomater.* **3**, 255–262 (2007).
- Sepulveda, P., Jones, J. R. & Hench, L. L. Bioactive sol-gel foams for tissue repair. *J. Biomed. Res.* **49**, 340–348 (2002).
- Regi, C. V., Vallet-Regi, M. & Rodriguez Lorenzo, L. M. Preparation and in vitro of hydroxyapatite/solgel glass biphasic material. *Biomaterial* **23**, 1865–1872 (2002).
- Dimitriev, Y., Ivanova, Y. & Iordanova, R. History of sol-gel science and technology. *J. Uni. Chem. Tech. and Metall.* **43**, 181–192 (2008).
- Hench, L. L. Sol-gel materials for bioceramic applications. *Curr. Opin. Solid State Mater. Sci.* **2**, 604–610 (1997).
- Martin, R. A. Characterizing the hierarchical structures of bioactive sol-gel silicate glass and hybrid scaffolds for bone regeneration. *Phil. Trans. Royal Soc. A* **28**, 1422–1443 (2012).
- Kaur, G. *et al.* A review of bioactive glasses: Their structure, properties, fabrication, and apatite formation. *J. Biomed. Mater. Res.* **A 102** (1), 254–274 (2014).
- Saravanapavan, P. & Hench, L. L. Low-temperature synthesis, structure, and bioactivity of gel-derived glasses in the binary CaO–SiO₂ system. *J. Biomed. Mater. Res.* **54**, 608–618 (2001).
- Fu, Q., Rahaman, M. N., Bal, B. S., Brown, R. F. & Day, D. E. Mechanical and in vitro performance of 13–93 bioactive glass scaffolds prepared by a polymer foam replication technique. *Acta Biomater.* **4**, 1854–1864 (2008).
- Ma, J., Chen, C. Z., Wang, D. G. & Meng, X. G. In vitro degradability and bioactivity of mesoporous CaO–MgO–P₂O₅–SiO₂ glasses synthesized by sol-gel method. *J. Sol-Gel Sci. Tech.* **54**, 69–76 (2010).
- Wang, X. P., Li, X., Ito, A. & Sogo, Y. Synthesis and characterization of hierarchically macroporous and mesoporous CaO–MO–SiO₂–P(2)O(5) (M = Mg, Zn, Sr) bioactive glass scaffolds. *Acta Biomater.* **7**, 638–644 (2011).
- Branda, F., Arcobello-Varlese, F., Costantini, A. & Luciani, G. Effect of the substitution of M₂O₃ (M = La, Y, In, Ga, Al) for CaO on the bioactivity of 2.5CaO.2SiO₂ glass. *Biomaterials* **23**, 711–716 (2002).
- Singh, K., Bala, I. & Kumar, V. Structural, optical and bioactive properties of calcium borosilicate glasses. *Ceram Int* **35**, 3401–3406 (2009).
- Bellantone, M., Williams, H. D. & Hench, L. L. Broad-spectrum bactericidal activity of Ag₂O-doped bioactive glass. *Antimicrob. Agents Chemother.* **46**, 1940–1945 (2002).
- Thamaraiselvi, T. V. & Rajeswar, S. Biological Evaluation of Bioceramic Materials - A Review. *Trends Biomater. Artif. Organs* **18**, 9–17 (2004).
- Aina, V., Malavasi, G., FiorioPla, A., Munaron, L. & Morterra, C. Zinc-containing bioactive glasses: Surface reactivity and behaviour towards endothelial cells. *Acta Biomater.* **5**, 1211–1222 (2009).
- Du, R. N., Chang, J., Ni, S. Y. & Zhai, W. Y. Characterization and in vitro bioactivity of zinc-containing bioactive glass and glass-ceramics. *J. Biomater. Appl.* **20**, 341–360 (2006).
- Jaroach, D. B. & Cluppper, D. C. Modulation of zinc release from bioactive sol-gel derived SiO₂-CaO-ZnO glasses and ceramics. *J. Biomed Mater Res* **82A**, 575–588 (2007).
- Varmette, E. A., Nowalk, J. R., Flick, L. M. & Hall, M. M. Abrogation of the inflammatory response in LPS stimulated RAW 264.7 murine macrophages by



- Zn- and Cu-doped bioactive sol-gel glasses. *J Biomed Mater Res* **90A**, 317–325 (2009).
29. Cousins, R. J. A role of zinc in the regulation of gene expression. *Proc. Nutr. Soc.* **57**, 307–311 (1998).
 30. Lang, C. *et al.* Anti-inflammatory effects of zinc and alterations in zinc transporter mRNA in mouse models of allergic inflammation. *Am. J. Physiol. Lung Cell Mol. Physiol.* **292**, L577–L584 (2007).
 31. El-Kady, A. M. & Ali, A. F. Fabrication and characterization of ZnO modified bioactive glass nanoparticles. *Cera. Inter.* **38**, 1195–1204 (2012).
 32. Courtheoux, L., Lao, J., Nedelec, J. M. & Jallot, E. Controlled bioactivity in zinc-doped sol-gel-derived binary bioactive glasses. *J. Phys. Chem. C* **112**, 13663–13667 (2008).
 33. Yamaguchi, M. Role of zinc in bone formation and bone resorption. *J. Trace Elem. Exp. Med.* **11**, 119–135 (1998).
 34. Oki, A., Parveen, B., Hossain, S., Adeniji, S. & Donahue, H. Preparation and in vitro bioactivity of zinc containing sol-gel-derived bioglass materials. *J. Biomed. Mater. Res.* **A69**, 216–221 (2004).
 35. Bettger, W. J. & O'Dell, B. L. Physiological roles of zinc in the plasma membrane of mammalian cells. *J. Nutr. Biochem.* **4**, 194–207 (1993).
 36. Huang, W. H., Day, D. E., Kittiratanapiboon, K. & Rahaman, M. N. Kinetics and mechanisms of the conversion of silicate (45 S5), borate, and borosilicate glasses to hydroxyapatite in dilute phosphate solutions. *J. Mater. Sci. Mater. Med.* **17**, 583–596 (2006).
 37. Lahl, N., Singh, K., Singheiser, L., Hilpert, K. & Bahadur, D. Crystallisation kinetics AO- Al₂O₃-SiO₂-B₂O₃ glasses (A = Ba, Ca, Mg). *J. Mat. Sci.* **35**, 3089–3096 (2000).
 38. Liang, W. *et al.* Bioactive borate glass scaffold for bone tissue engineering. *J. Non-Cryst. Solids* **354**, 1690–1696 (2008).
 39. Saranti, A., Koutselas, I. & Karakassides, M. A. Bioactive glasses in the system CaO-B₂O₃-P₂O₅: preparation, structural study and in vitro evaluation. *J. Non-Cryst. Solids* **352**, 390–398 (2006).
 40. Lee, J. H. *et al.* In vivo study of novel biodegradable and osteoconductive CaO-SiO₂-B₂O₃ glass-ceramics. *J. Biomed. Mater. Res.* **77A**, 362–369 (2006).
 41. Valliant, E. M., Turdean-Ionescu, C. A., Hanna, J. V., Smith, M. E. & Jones, J. R. *J. Mater. Chem.* **22**, 1613–1619 (2012).
 42. De Oliveira, A. A. R. *et al.* Synthesis, characterization and cytocompatibility of spherical bioactive glass nanoparticles for potential hard tissue engineering applications. *Biomed. Mater.* **8**, 025011–25 (2011).
 43. Wnek, W. J. An analysis of the dependence of the zeta potential and surface charge on surfactant concentration, ionic strength, and pH. *J. Coll. Inter. Sci.* **60**, 361–375 (1977).
 44. Michael, M. D., Mikowski, A., Lepienski, C. M., Foerster, C. E. & Serbena, F. C. High temperature microhardness of soda-lime glass. *J. Non-Crystal. Solids* **348**, 131–138 (2004).
 45. Rehman, M. N. *et al.* Bioactive glass in tissue engineering. *Acta Biomat.* **7**, 2355–2373 (2011).
 46. Ranjan, A. *et al.* Antibacterial efficacy of core-shell nanostructures encapsulating gentamicin against an in vivo intracellular Salmonella model. *Int. J. Nanomed.* **4**, 289–297 (2009).
 47. Oudadesse, H. *et al.* Apatite forming ability and cytocompatibility of pure and Zn-doped bioactive glasses. *Biomed. Mater.* **6**, 035006–15 (2011).
 48. Yang, X. *et al.* Incorporation of B₂O₃ in CaO-SiO₂-P₂O₅ bioactive glass system for improving strength of low-temperature co-fired porous glass ceramics. *J. Non-Cryst. Solids* **358**, 1171–1179 (2012).
 49. Kaur, G., Sharma, P., Kumar, V. & Singh, K. Assessment of *in-vitro* bioactivity of SiO₂-BaO-ZnO-B₂O₃-Al₂O₃ glasses: An optico-analytical approach. *Mater. Sci. & Engg. C* **32**, 1941–1947 (2012).
 50. Makino, K. *et al.* Temperature- and ionic strength-induced conformational changes in the lipid head group region of liposomes as suggested by zeta potential data. *Biophys. Chem.* **41**, 175–183 (1991).
 51. Wnek, W. J. An analysis of the dependence of the zeta potential and surface charge on surfactant concentration, ionic strength, and pH. *J. Colloid Inter. Sci.* **60**, 361–375 (1997).
 52. Kokubo, T. Design of bioactive bone substitutes based on biomineralization process. *Mat. Sci. Eng. C* **25**, 97–104 (2005).
 53. Kokubo, T., Kim, H. M. & Kawashita, M. Novel bioactive materials with different mechanical properties. *Biomater.* **24**, 2161–75 (2003).
 54. Doostmohammadi, A. *et al.* A comparative physico-chemical study of bioactive glass and bone-derived hydroxyapatite. *Ceram. Int.* **37**, 2311–16 (2011).
 55. Regi, M. V. Ceramics for medical applications. *J. Chem. Soc. Dalton Trans.* **2**, 97–108 (2001).
 56. LeGeros, R. Z. & LeGeros, J. P. Phosphate minerals in human tissues. (Eds. Nriagu, J. O. & Moore, P. B.), 351–385, (Springer-Verlag, Berlin, 1984).
 57. Tas, A. C. Synthesis of Biomimetic Ca-Hydroxyapatite Powders at 37°C in Synthetic Body Fluids. *Biomater.* **21**, 1429–1438 (2000).

Acknowledgments

Authors are thankful to CIES, Washington D.C. for the financial assistance. One of the authors (GK) is thankful to Dr. O.P. Pandey and Dr. K. Singh, Thapar University, India for their consistent support and guidance. G.K. is also thankful to Dr. Vishal Kumar and Yujie Cheng, Virginia Tech, USA for their valuable suggestions and help during the course of the work.

Author contributions

All authors have reviewed the manuscript. G.K. is the first author and wrote the main manuscript and prepared the figures. She performed SEM, XRD, mechanical measurements and thermal studies. G.P. decided the composition for these studies and designed the experiments. Furthermore, he gave his expert comments after every study. D.H. helped in analyzing the results of zeta potential and particle size measurements. H.A. helped in pH measurements. N.S. and G.K. did cytotoxicity, live-dead cell studies and prepared figures 5, 6(a–b) and 7.

Additional information

Competing financial interests: The authors declare no competing financial interests.

How to cite this article: Kaur, G. *et al.* Synthesis, cytotoxicity, and hydroxyapatite formation in 27-Tris-SBF for sol-gel based CaO-P₂O₅-SiO₂-B₂O₃-ZnO bioactive glasses. *Sci. Rep.* **4**, 4392; DOI:10.1038/srep04392 (2014).



This work is licensed under a Creative Commons Attribution-NonCommercial-NoDerivs 3.0 Unported license. To view a copy of this license, visit <http://creativecommons.org/licenses/by-nc-nd/3.0>